

COMPUTER SIMULATION OF A WOODSTOVE THERMAL STORAGE SYSTEM

Y. H. ZURIGAT and A. J. GHAJAR

School of Mechanical and Aerospace Engineering, Oklahoma State University,
Stillwater, OK 74078, U.S.A.

(Received 7 August 1985)

Abstract—A simulation program has been developed to study the use of thermal storage for residential woodstoves. The behavior of thermal storage under the woodstove operating conditions, i.e. variable heat flux, was well-represented, and the parameters affecting its performance in both charge and discharge modes were qualitatively identified. The analysis showed that the spacing between the thermal storage mass and the stove significantly affects the room temperature during the charge mode, while the thickness of the thermal storage mass has a moderate effect during the discharge mode. Simulations with different stove sizes established an upper limit on thermal mass thickness of about 11" and a lower limit on spacing of about 3". The program is capable of selecting the exact combination of thickness and spacing for a given space.

Thermal storage Woodstove Computer simulation Energy conservation Modeling

NOMENCLATURE

A = Area
 b = Storage mass wall thickness
 Bi = Biot number, $Bi = h_c \Delta x / k$
 C = Specific heat
 F = Radiation shape factor
 Fo = Fourier number, $Fo = \alpha \Delta \tau / (\Delta x)^2$
 Gr = Grashof number, $Gr = g \beta (T_w - T_\infty) L^3 \rho^2 / \mu^2$
 g = Acceleration of gravity
 h = Average heat transfer coefficient
 k = Thermal conductivity
 m = Mass
 Nu = Average Nusselt number, $Nu = hL/k$
 Pr = Prandtl number, $Pr = \mu C_p / k$
 Q_{FLR} = Floor rate of heat loss
 Q_{INF} = Infiltration rate of heat loss, $Q_{INF} = \rho V C_p (t_i - t_o)$
 Q_{LOSS} = Space rate of heat loss
 Q_{LP} = Heat sources (people, lights etc.)
 Q_{STG} = Heat storage or discharge rate
 Q_{STV} = Stove useful heat output rate
 R = Dimensionless number analogous to Biot number, $R = h_c \Delta x / k$
 T = Temperature
 T_f = Fluid temperature, $T_f = (T_w + T_{st})/2$
 T_{st} = Stove temperature
 T_w = Concrete wall temperature
 T_∞ = Temperature of undisturbed air
 t_i = Indoor temperature
 t_o = Outdoor temperature
 t_{ov} = Temperature of outdoor space adjacent to j th side of given space, used in equations (4) and (5)
 U_{jn} = Thermal conductance of n th surface of j th side of given space, used in equations (4) and (5)
 V = Air flow rate
 α = Thermal diffusivity, $\alpha = k / \rho C_p$
 β = Coefficient of thermal expansion
 σ = Stefan-Boltzmann constant
 ϵ = Total hemispherical emissivity
 δ = Spacing between stove and storage wall
 μ = Absolute viscosity
 ρ = Density
 τ = Time

Subscripts

c = Convection
 p = At constant pressure
 r = Radiation
 w = Evaluated at the wall
' = Future value

1. INTRODUCTION

Modern airtight woodstoves with efficiencies of 50–60%, excellent temperature regulation and with burn cycles of 8 h or longer have become quite popular. This extended burn cycle is achieved by operating the stove under starved air conditions, i.e. imposing a significant restriction on the combustion air supply. Operating the stove in this manner produces cold fire which has a distinct disadvantage to hot-fire operation.

In cold-fire operation, complete combustion of the wood's gaseous by-products is not possible. These volatile gases account for 30–60% of the wood's fuel value and ignite only when the fire is hot, $\geq 1100^\circ\text{F}$ [1]. Unburned, these gases escape up the cool exhaust, condensing into a liquid which eventually dries to a hard crust known as creosote. Creosote formation constitutes a fire hazard because it is highly combustible, and when it ignites under accidental hot fire, flue gas temperatures $> 2000^\circ\text{F}$ occur [2]. Creosote is the cause of most chimney fires.

Cold-fire operation also causes excessive pollution. Under starved air conditions, large quantities of CO and smoke particles are emitted. Moreover, a recent study by Monsanto Research Corp. [3] showed that airtight woodstoves are a major producer of polycyclic organic matter (POM) which is toxic. The

results of that study suggest that the rate of POM emission from residential combustion of wood is significantly higher (on a per joule basis) than from residential oil or gas combustion.

Examining the above problems, it is clear that the solution lies in stove operation. The stove should maintain a high combustion temperature, whenever it is in operation. On the other hand a prolonged fire of that intensity would soon overheat the living area and consume large quantities of wood. The solution to this last problem calls for thermal storage. The energy, far in excess of the room's heat loss over a shortened burn cycle, should be stored and then released when demanded by a drop in the room temperature.

Recently, thermal storage has been proposed as a solution to the problems associated with wood-burning stoves [4, 5]. A recent experimental study by Pilcher and Ghajar [2] showed that thermal storage enhances woodstoves' combustion efficiency and reduces pollution and creosote formation. That study constituted Phase II of a two-phase study conducted at the Oklahoma State University.

In this study (Phase I) a computer simulation of a woodstove thermal storage system (TSS) was conducted to obtain information for sizing the proposed system through heat transfer systems analysis. Information on the basic dimensions of the TSS and the parameters governing its performance were obtained.

The specific objectives of this study were to develop a computer program to predict:

- (1) the behavior of the TSS under woodstove operating conditions, i.e. variable heat flux;

and

- (2) the parameters affecting the TSS performance in both charge and discharge modes.

The TSS physical model is a concrete wall surrounding the stove on three sides, built up to the height of the stove and placed a certain distance from the stove (see Fig. 1). The choice of concrete as a thermal storage medium is due to its availability and low cost. Other materials can be used by inputting their properties into the simulation program.

2. ANALYSIS

The objective of this analysis was to determine the transient indoor temperature profile as a function of woodstove heat output and the thermal storage mass dimensions. Then, the effects of the storage mass parameters were determined by the corresponding indoor temperature profiles.

From an energy balance on the given space:

$$Q_{\text{LOSS}} = Q_{\text{NET}} = Q_{\text{STV}} - Q_{\text{STG}} \quad (1)$$

The stove useful heat output Q_{STV} in equation (1) is governed by the stove surface temperature T_{st} at any

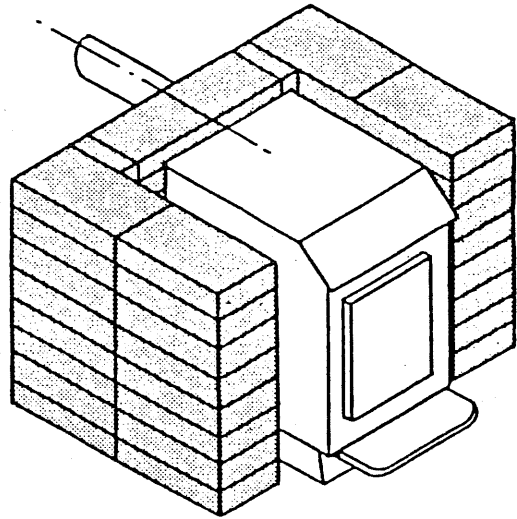


Fig. 1. Woodstove and concrete thermal mass storage system.

instant of time. T_{st} can be obtained experimentally or assumed in the simulation. Q_{STV} is calculated using the radiation and free-convection relations [see the Appendix, equations (A.2)–(A.6)]. The storage rate Q_{STG} is governed totally by the transient temperature profile across the storage mass which was obtained by solving the heat conduction equation

$$\frac{\partial^2 T}{\partial x^2} + \frac{\partial^2 T}{\partial y^2} = \frac{1}{\alpha} \frac{\partial T}{\partial \tau} \quad (2)$$

numerically using an explicit finite-difference method [6] (see the Appendix). The storage rate was then determined by

$$Q_{\text{STG}} = mC \frac{\partial T}{\partial \tau} \quad (3)$$

Since the space heat loss Q_{LOSS} is a function of indoor and outdoor temperatures, the space structure thermal resistance values and the infiltration of outside air into the space, Q_{LOSS} can be expressed as [7]

$$Q_{\text{LOSS}} = \sum_{j=1}^K \sum_{n=1}^N U_{jn} A_{jn} (t_i - t_{oj}) + Q_{\text{FLR}} + Q_{\text{INF}} - Q_{\text{LP}} \quad (4)$$

Then upon substitution of equation (4) in equation (1) and solving for t_i we get

$$t_i = \left[Q_{\text{STV}} - Q_{\text{STG}} - Q_{\text{FLR}} - \rho V C_p t_o + Q_{\text{LP}} + \sum_{j=1}^K t_{oj} \sum_{n=1}^N U_{jn} A_{jn} \right] / \left[\sum_{j=1}^K \sum_{n=1}^N U_{jn} A_{jn} + \rho V C_p \right] \quad (5)$$

In the derivation of equation (5), the following simplifying assumptions were made:

- (1) the net heat output Q_{NET} is distributed uniformly over the space;
- (2) there is no time lag for the Q_{NET} to interact with the indoor air;

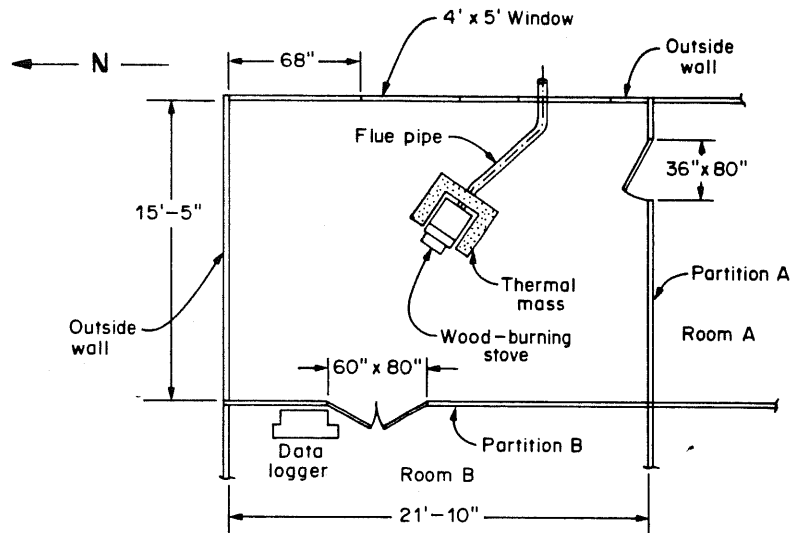


Fig. 2. Experiment room—floor plan.

(3) the room structure solar gain is negligible;
and

(4) the infiltration is constant.

Note that in equation (5), Q_{STG} may have a positive sign (charge) or a negative sign (discharge).

3. EXPERIMENTS

In order to check the validity of the analysis and the simulation program, a SIERA brand woodstove was installed in a room with a ceiling height of 11.6 ft and dimensions as indicated in Fig. 2. For details of the experimental setup and procedure refer to Pilcher and Ghajar [2]. The temperatures of the firebox surfaces and stove pipe were recorded along with the indoor and outdoor temperatures. A total of 39 thermocouples were used, 17 of them were used to measure the stove surface and pipe temperatures at different locations. The readings were taken at 15 min time intervals. Then, an equivalent temperature for each surface at each time interval was found by averaging the measured temperatures for that surface. Figure 3 shows the results. The temperature profile across the thermal mass was obtained using a total of 18 thermocouples. A total of 10 experiments were conducted, and they all showed a similar behavior. The outdoor temperature was between 12 and 14°F during the experiment, and the temperatures in the adjacent rooms were 34–36°F in room A and 40–48°F in room B (see Fig. 2). The experiments were carried out with 7.5" of thermal mass and 3" of spacing between the thermal and the stove.

4. INPUT DATA

The input data required for the simulation were the space dimensions, structure thermal resistance values,

the stove dimensions, the thermal properties of concrete, the radiative properties of both concrete and the stove, the transient temperature profiles of the stove surfaces and the outdoor transient temperature profile. For details refer to Zurigat [8].

5. RESULTS AND DISCUSSION

The calculated indoor temperature profile (Fig. 3) indicates that the heat transfer model used is accurate. A complete agreement between the calculated and experimental indoor temperature profiles cannot be achieved due to the first two assumptions made in Section 2 and the fact that many of the variables involved cannot be estimated very accurately. Despite this, it is clear that the trends are well-represented, as shown in Fig. 3, and the simulation using the present analysis faithfully represents the relative changes in the heat transfer system parameters.

With this in mind, the program then simulated the system performance under different thermal mass parameters (thickness and spacing) for different stove sizes. The following results were established:

1. The thermal mass (concrete) acts as what the authors like to call a "thermal accumulator", that is in direct interaction with the heat transfer system. The thermal mass absorbs the stove heat output at proportional rates and dissipates heat as a drop in stove heat flux or room temperature occurs (see Figs 3 and 4). This behavior explains the storage mass capability of preventing overheating the space due to high stove surface temperature (see Fig. 3).
2. The thermal mass thickness (TMT) has less effect on the indoor temperature during the charge mode relative to that in the discharge mode. This can be seen when comparing the relative changes in indoor temperature with the

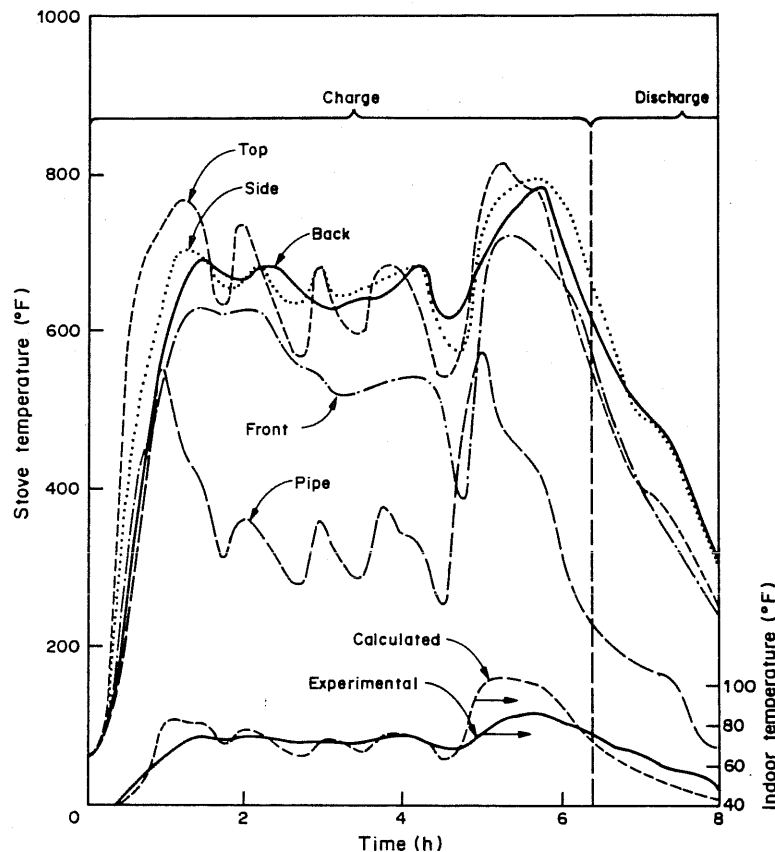


Fig. 3. Experimental data and calculated indoor temperature profile.

TMT in charge and discharge modes (see Fig. 4). The fact that a larger TMT causes more heat storage and, accordingly, less stove heat output into the space during the charge mode holds true up to a certain TMT, after which the heat storage efficiency (see Fig. 5) will experience a negligible increase. This establishes an upper limit on the TMT of about 11", no matter what the stove temperature might be (results for a 10 and 30% reduction in stove temperature established this limit [8]). On the other hand, a thin storage mass becomes more active in the heat transfer system, i.e. it responds quickly to the changes in the stove and indoor temperatures. The lower limit on the TMT is established by the required discharge rate. For example, 7.5" of TMT gives a higher discharge rate for a longer time compared to 5.5" of TMT (see Fig. 6).

3. The spacing between the stove and the thermal mass, δ , has a significant effect on the indoor temperature during the charge mode with a negligible effect during the discharge mode (see Figs 7 and 8). This follows from the change in the radiation shape factors between the stove, the thermal mass and the space, the increase in the free convection (see the Appendix, Fig. A1),

and the relative change in the storage efficiency with the spacing (see Fig. 9). This result is in good agreement with the experiments of Laughlin [9] (see Fig. 10).

Note that the experimental results of Pilcher and Ghajar [2] showed that the lower the spacing, the higher the combustion temperature. In this simulation, this result cannot be predicted. A more advanced model, involving the variables governing the wood-combustion process inside the firebox, is required. On the other hand, it can be argued that the reduction in stove heat output into the space with the decrease in spacing results in an increase in the stove surface temperature (see Fig. 7 [2]) which leads to an increase in the rate of wood pyrolysis and combustion temperature thereafter. It is obvious that, due to the system geometry, a change in spacing by $|\Delta\delta|$ causes a change in the thermal storage mass by

$$\Delta m =$$

$$4|\Delta\delta| \times \text{stove height} \times \text{TMT} \times \text{concrete density.}$$

In practice, the minimum spacing is not determined by the heat transfer criterion alone but rather by the safety criterion, i.e. allowing adequate access for periodic cleaning of dust and/or any flammable matter that may fall in between the stove and the

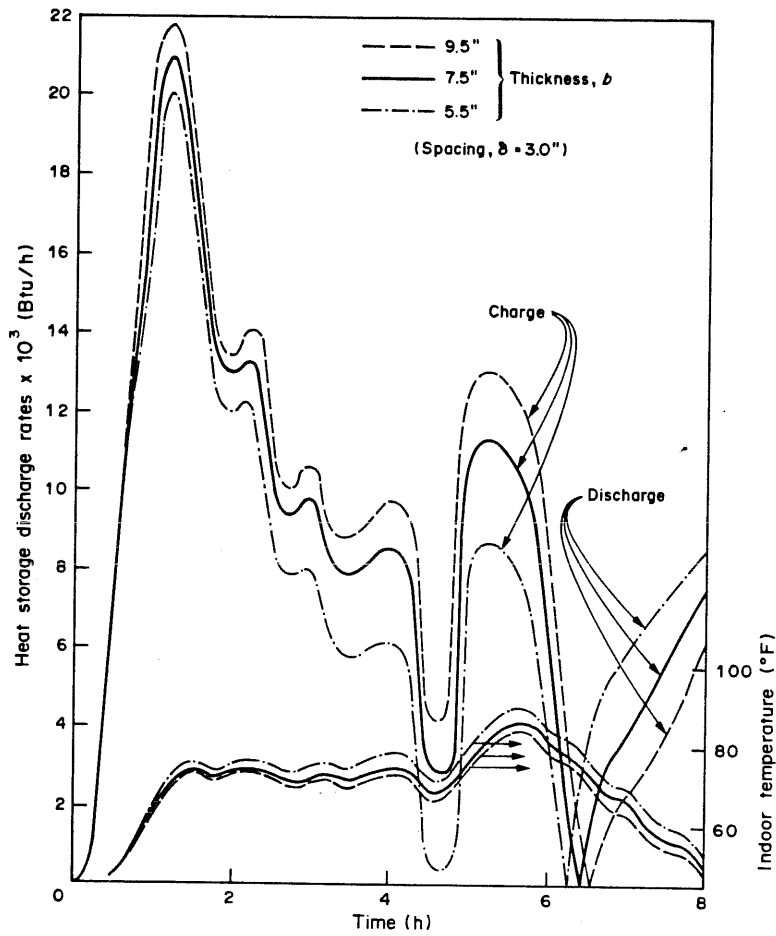


Fig. 4. Effect of TMT on indoor temperature and heat storage and discharge rates (constant spacing).

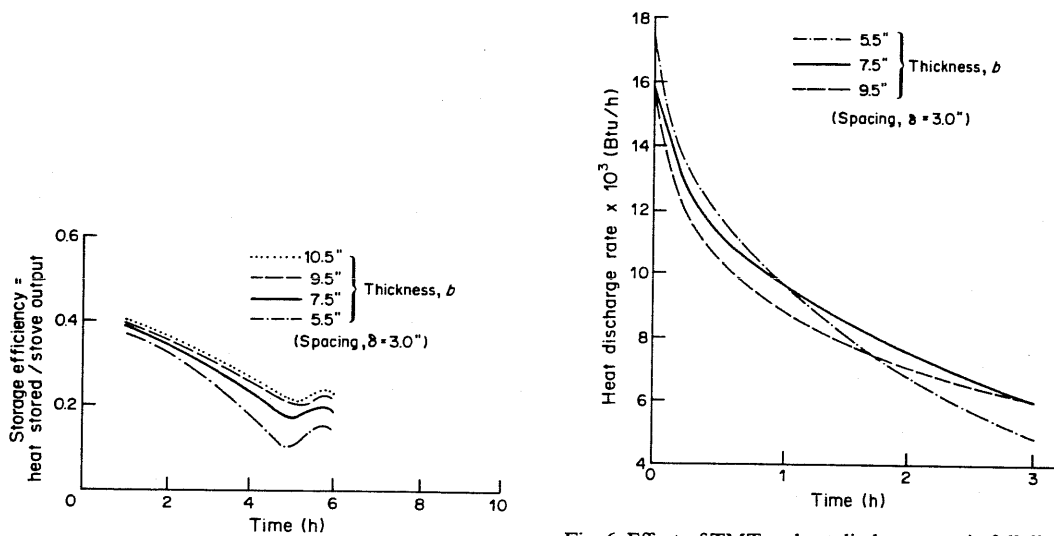


Fig. 5. Effect of TMT on heat storage efficiency (constant spacing).

Fig. 6. Effect of TMT on heat discharge rate in full discharge mode (full discharge mode means that the stove and space are at the same temperature) (constant spacing).

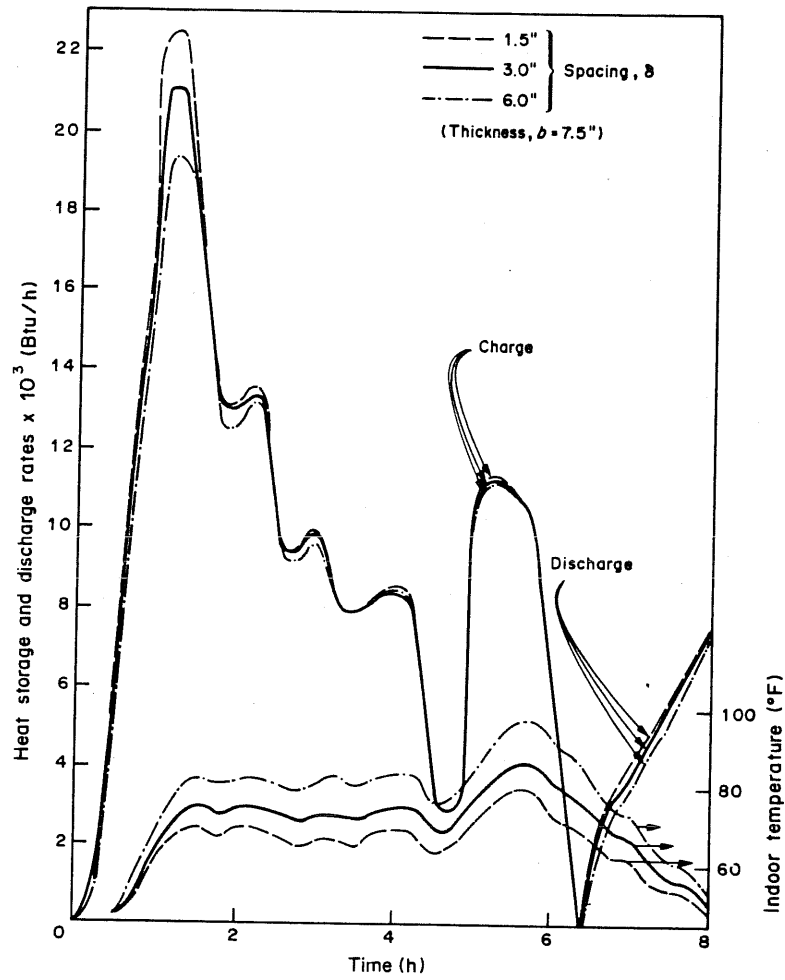


Fig. 7. Effect of spacing on indoor temperature and heat storage and discharge rates (constant thickness).

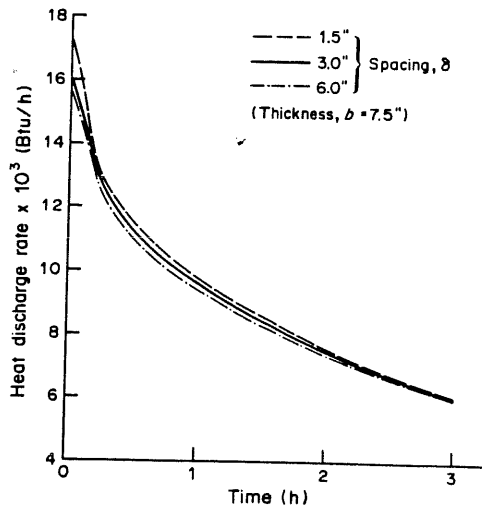


Fig. 8. Effect of spacing on discharge rate in fully discharge mode (constant thickness).

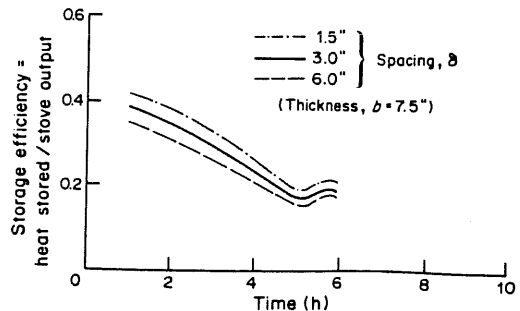


Fig. 9. Effect of spacing on heat storage efficiency (constant thickness).

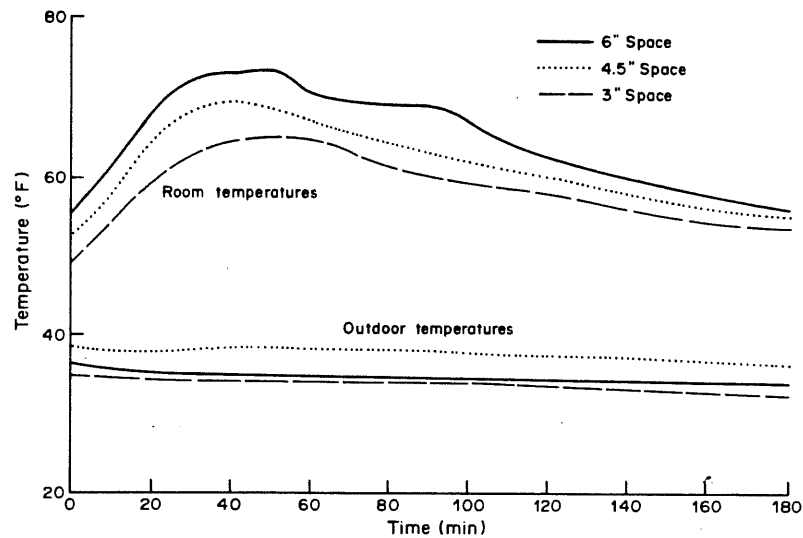


Fig. 10. Room temperature vs time for various mass spacings [9].

thermal mass. A minimum spacing of 3" satisfies these criteria. As seen from Figs 7, 9 and 10, the indoor temperature during the charge mode can be controlled by varying the spacing, δ .

The simulation program developed in this study was shown to have the capability of predicting variations in the indoor temperature for given system parameters (i.e. thermal mass dimensions, stove surface temperatures, space variables etc.). Thus, the program can be used as a tool for sizing the thermal storage system.

A stove surface temperature characterization as to the type of wood and draft settings is necessary. The series of experiments conducted at this university indicate that such characterization (within a reasonable accuracy) is possible despite the many variables governing the wood-combustion process in woodstoves. Further work in this area is necessary.

6. CONCLUSIONS

Emphasis needs to be placed on the development of effective measures to ensure complete combustion in wood-burning stoves so that the desired energy efficiency can be obtained in a safe and environmentally acceptable manner. In this study, the use of thermal storage has been investigated to aid in achieving this goal. The results of the simulation presented in this paper are in good agreement with experiments, demonstrating thereby the predictive capability of the analysis used. It was shown that the simulation program developed in this study is an effective tool for sizing the proposed system through simulation of the heat transfer system comprising stove, thermal mass and space based on the three basic modes of heat transfer.

Acknowledgement—The assistance of Mr Ken Pilcher with the experimental setup is gratefully acknowledged.

REFERENCES

1. J. W. Shelton, *Solid Fuel Encyclopedia*. Garden Way Publishing, Charlotte, Vt (1983).
2. K. R. Pilcher and A. J. Ghajar, *Energy* **10**, 1151 (1985).
3. D. G. DeAngelis, D. S. Ruffin and R. B. Resnik, Report EPA-600/7-80-040, Monsanto Research Corp., Dayton, Ohio (1980).
4. *Mother Earth News* Jan./Feb. 99 (1981).
5. S. Klapper, *Renewable Energy News: New Roots for the Northeast Magazine* Jan./Feb., 28 (1980).
6. D. R. Croft and D. G. Lilley, *Heat Transfer Calculations using Finite Difference Equations*. Applied Science Publishers, London (1977).
7. F. C. McQuiston and J. D. Parker, *Heating, Ventilating, and Air Conditioning. Analysis and Design*, 2nd edn. Wiley, New York (1982).
8. Y. H. Zurigat, M. S. Report, Mechanical and Aerospace engineering Dept, Oklahoma State Univ., Stillwater, Okla. (1984).
9. G. Laughlin, Internal Report, Mechanical and Aerospace Engineering Dept, Oklahoma State Univ., Stillwater, Okla. (1984).
10. J. A. Duffie and W. A. Beckman, *Solar Engineering of Thermal Processes*. Wiley, New York (1980).
11. A. J. Chapman, *Heat Transfer*, 3rd edn. Macmillan, New York (1974).
12. J. Sucec, *Heat Transfer*. Simon & Schuster, New York (1975).
13. E. M. Sparrow and J. L. Gregg, *Trans. ASME* **80**, 879 (1958).

APPENDIX

Storage mass transient temperature profile

In order to find the transient temperature profile across the storage mass, equation (2) with the appropriate boundary conditions was solved for the 1-D and 2-D cases. The numerical results of the calculated heat storage and discharge rates for the 2-D case were 9% less than those for the 1-D case. Therefore, only the 1-D analysis will be presented here. For the 2-D analysis refer to Zurigat [8].

Development of the theoretical model. The analysis presented here is for one side of the storage wall as shown in Fig. A1. Due to similarities, the same analysis is applicable to the other sides of the storage wall.

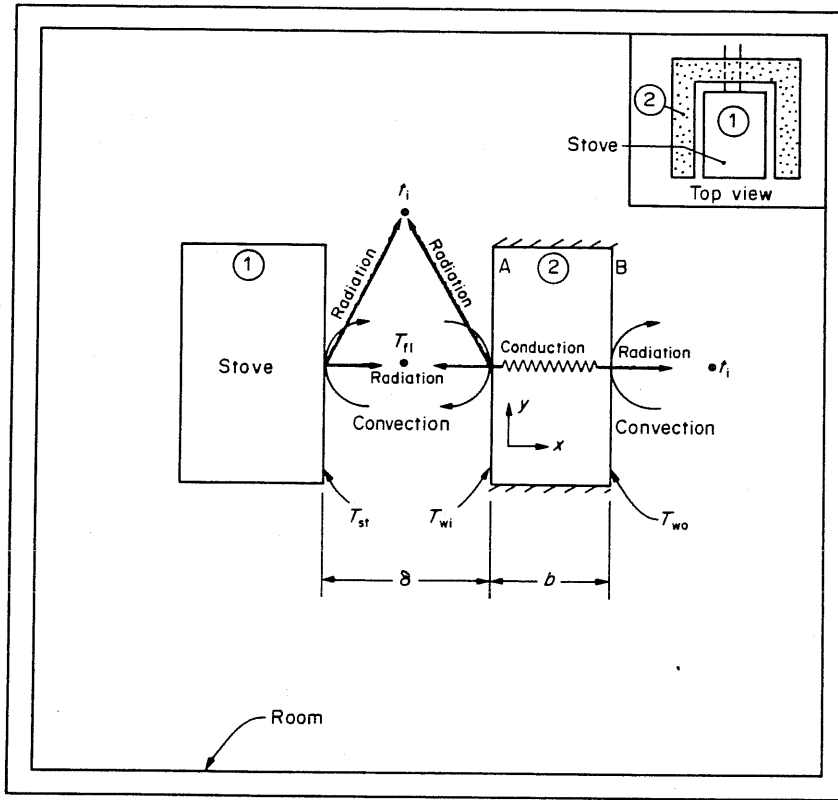


Fig. A1. Thermal mass boundary conditions.

Under the following assumptions:

- (1) the heat loss from the upper, lower and front edges of the storage wall is negligible—this is justified by the fact that the areas of the edges are relatively small, and the lower edge is placed on an insulating sheet

and

- (2) the temperature variations are significant only in the x -direction (across the storage wall),

a 1-D analysis can be conducted with good accuracy. Thus, equation (2) reduces to

$$\frac{\partial^2 T}{\partial x^2} = \frac{1}{\alpha} \frac{\partial T}{\partial \tau} \quad (A.1)$$

The boundary and initial conditions imposed on the storage wall are (see Fig. A1) as follows.

- (1) On face A, we have: (a) radiation heat transfer to the space at indoor temperature t_i ; (b) radiation heat exchange with the stove at temperature T_{st} ; and (c) convection exchange with the fluid (air) at an average temperature of $T_{fl} = (T_{wi} + T_{st})/2$.
- (2) On face B, we have: (a) radiation heat transfer to the space at indoor temperature t_i ; and (b) convection exchange with the indoor air at temperature t_i .
- (3) The initial temperatures (at time $\tau = 0$) are those of the space. The radiation heat exchange between any two surfaces is given by [10]

$$Q_{r1} = A_1 h_r (T_2 - T_1) \quad (A.2)$$

where

$$h_r = \frac{\sigma (T_2^2 + T_1^2) (T_2 + T_1)}{\frac{1 - \epsilon_1}{\epsilon_1} + \frac{1}{F_{1-2}} + \frac{1 - \epsilon_2}{\epsilon_2} \frac{A_1}{A_2}} \quad (A.3)$$

The radiation heat transfer coefficient h_r for the case of heat exchange with the space (first boundary condition on faces A and B) can be found from equation (A.3) to be

$$h_r = \epsilon_1 \sigma (T_2^2 + T_1^2) (T_2 + T_1) \quad (A.4)$$

The convection heat transfer between any surface at temperature T_w and the fluid at temperature T_{fl} is given by

$$Q_c = h_c A_w (T_w - T_{fl}) \quad (A.5)$$

where the convection heat transfer coefficient h_c was determined by the free-convection heat transfer correlations given in Table 1 [8, 11, 12]. The physical properties in the heat transfer correlations were evaluated at the reference temperature T_r proposed by Sparrow and Gregg [13]:

$$T_r = T_w - 0.38 (T_w - T_{fl}) \quad (A.6)$$

Equations (A.2)–(A.6) include nonlinear terms such as, the convective and radiative heat transfer coefficients, and

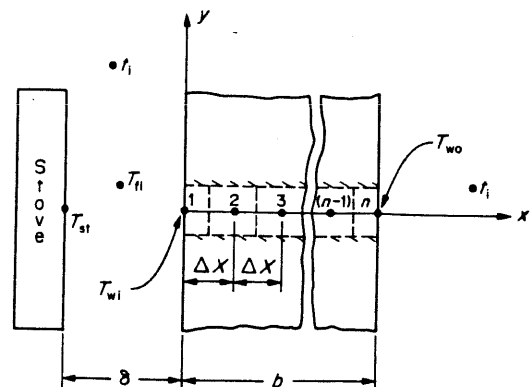


Fig. A2. Finite-difference network (1-D).

Table 1. Free-convection heat transfer correlations

(GrPr) Range	Correlation	Reference
(1) Vertical plates		
$0 < \text{GrPr} < 10^4$	$\text{Nu} = 1.09 (\text{GrPr})^{0.185}$	[8]*
$10^4 < \text{GrPr} < 10^9$	$\text{Nu} = 0.59 (\text{GrPr})^{0.25}$	[12]
$10^9 < \text{GrPr} < 10^{12}$	$\text{Nu} = 0.13 (\text{GrPr})^{1/3}$	[12]
$10^{10} < \text{Gr}$	$\text{Nu} = 0.0246 \text{Gr}^{0.4} \left[\frac{\text{Pr}^{7/15}}{(1 + 0.494 \text{Pr}^{2/3})^{0.4}} \right]$	[12]
(2) Heated horizontal plates facing upward		
$10^4 < \text{GrPr} < 10^8$	$\text{Nu} = 0.54 (\text{GrPr})^{0.25}$	[12]
$10^8 < \text{GrPr}$	$\text{Nu} = 0.14 (\text{GrPr})^{1/3}$	[12]

*For the range $0 < \text{GrPr} < 10^4$, Chapman [11] recommended the use of a graph. The data of Nu vs (GrPr) obtained from Chapman [11] were correlated using a nonlinear least-squares fit.

the variable properties of air. As a result of these complexities, equation (A.1) could not be solved in closed form, and an explicit finite-difference formulation was adopted. This method of solution is presented next.

Finite-difference formulation. In order to develop the finite-difference equations, a network of nodes for the unknown temperatures was established (see Fig. A.2). The nodes were placed a distance Δx apart in the x -direction.

For the interior nodes, equation (A.1) can be replaced by

$$T'_K = \text{Fo}[T_{K-1} + T_{K+1} + T_K(1/\text{Fo} - 2)], \quad (\text{A.7})$$

with $K = 2, 3, \dots, n-1$.

For the boundary nodes 1 and n , with conduction, convection and radiation present, an energy balance on the control volume of width $\Delta x/2$, length Δy and depth Δz (where $\Delta x = \Delta y = \Delta z$) associated with each node gives:

$$\begin{aligned} \text{Time rate of change} & \quad \text{Rate of heat convected} \\ \text{of stored energy within} & = \text{into the control volume} \\ \text{the control volume} & \quad \text{by fluid at } T_f \\ & \quad \text{Rate of heat gain by} \\ & \quad \text{radiation from the stove} \\ & \quad + \text{and/or from the space} \\ & \quad \text{Rate of heat conducted} \\ & \quad + \text{into the control volume} \\ & \quad \text{from the adjacent node.} \end{aligned} \quad (\text{A.8})$$

Using equation (A.8) it can be shown that, for node 1, the temperature at time $(\tau + \Delta\tau)$ is given by

$$\begin{aligned} T'_1 = 2\text{Fo}[T_2 + \text{Bi}_1 T_f + R_1 T_{s1} + R_2 t_i \\ + T_1(1/2\text{Fo} - \text{Bi}_1 - R_1 - R_2 - 1)]. \end{aligned} \quad (\text{A.9})$$

In a similar way, for the boundary point n , the temperature T_n at time $(\tau + \Delta\tau)$ is

$$\begin{aligned} T'_n = 2\text{Fo}[T_{n-1} + \text{Bi}_n t_i + R_n t_i \\ + T_n(1/2\text{Fo} - \text{Bi}_n - R_n - 1)]. \end{aligned} \quad (\text{A.10})$$

Equations (A.7), (A.9) and (A.10) explicitly express the future temperatures at time $(\tau + \Delta\tau)$ in terms of known temperatures at time (τ) .

In obtaining the stability criterion, the most restrictive condition was found from equation (A.9) to be

$$[1/2\text{Fo} - \text{Bi}_1 - R_1 - R_2 - 1] \geq 0. \quad (\text{A.11})$$

Then, the Fourier number becomes

$$\text{Fo} \leq \frac{1}{2(\text{Bi}_1 + R_1 + R_2 + 1)}. \quad (\text{A.12})$$

For the given conditions, $\text{Fo} \leq 0.2$ was found to be safe for obtaining a stable solution.